GMR
The Original

MOLECULAR DOCKING AND COMPUTATIONAL INVESTIGATION OF MENTHA ROYLEANA PHYTOCHEMICALS TARGETING PROTEINS AND PATHWAYS INVOLVED IN GASTROINTESTINAL MOTILITY

Ali Jan[1], Syed Mahboob Alam[1], Imran Rabbani[2], Zubaida Umar zehri[1], Zaib-un-Nisa[3], Abid Hussain[4], Izhar Ullah[4]*, Saeeda Naseer[1]

[1]Department of Pharmacology and Therapeutics Basic Medical Science Institute JPMC Karachi, University of Karachi, Sindh Pakistan.
[2]Department of Pharmacy, Kohat University of Science and Technology, Kohat, KP, Pakistan.
[3]Governamnent College Women University, Sialkot Punjab Pakistan
[4]Department of Pharmacy, Faculty of Medical and Health Sciences University of Poonch Rawalakot, AJK, Pakistan.

ABSTRACT
Gastrointestinal motility disorders are linked with deregulated smooth muscle contraction controlled by important protein targets L-type voltage-gated calcium channel Cav1.2 and M3 muscarinic acetylcholine receptor. The current study focused on an integrated in silico approach to analyze the therapeutic potential of phytocompounds of *Mentha royleana* against these target proteins. A total of 20 compounds, identified by GCMS technique, were subjected to QSAR analysis, drug-likeness and toxicity filters, molecular docking, and density functional theory (DFT) analysis. The best performing QSAR model,among the used multiple machine learning algorithms, was found to be XGBoost which enabled effective prioritization of compounds based on predicted inhibitory activity (pIC50). Preliminary drug-likeness evaluation by Lipinski and Veber rules and safety screening helped in further prioritization of compounds. Molecular docking study revealed compound 1-[alpha-(1-Adamantyl)benzylidene]thiosemicarbazide (CPD1) having strong binding affinity scores(up to -9.7 kcal/mol) with both targets, supported by hydrogen and hydrophobic interactions. DFT technique provided understandings about electronic properties of ligands, with lowest HOMO-LUMO energy gap (4.719 eV) and highest dipole moment (5.943 D) was found for CPD1, supporting its higher reactivity and binding affinity. Drug-likeness analysis indicated favorable oral absorption while pharmacokinetic profiling exhibited acceptable ADMET properties for most lead compounds, though some compounds with predicted toxicity require optimization. Overall, the study emphasizes compound CPD1 as a promising lead drug candidate demonstrating a balance of predicted biological activity, binding interactions, and electronic stability. The study results have revealed that *M. royleana* is a beneficial source of bioactive phytocompounds with potential antispasmodic effect by dual inhibition of M3R receptor and Cav1.2 channel. This in silico framework demonstrates the pharmacological relevance of *M. royleana* and delivers a strong basis for further experimental validation of predicted findings and rational drug development for targeting gastrointestinal motility disorders.
KEYWORDS: *Mentha royleana*, Gastrointestinal motility disorders, Cav1.2, M3 muscarinic receptor, Molecular Docking, QSAR

INTRODUCTION

Hyperactive gut disorders and gastric ulcers are among the highly prevalence gastrointestinal diseases which are associated with impaired GUT motility, chronic inflammation and oxidative stress (Hu et al. 2024; Flaskerud 2020). These diseases put a huge burden on the health care system globally and have affected the quality of life of the people globally (Milivojevic and Milosavljevic 2020; Barkun and Leontiadis 2010). Currently available medications are associated with side effects and limited efficacy which warrant discovery of more safe and effective agents for gastrointestinal disorders (McQuaid 2018; Narayanan et al. 2018). Natural products are of immense importance in the field of medicine, as they have historically served as the foundation for many therapeutic agents (Frevel and Nihan 2012). Plants can be explored effectively to find out therapeutic agents' alternative to synthetic drugs. Almost 25 % of the universally prescribed drugs are obtained from plants (Farnsworth et al. 1985).

Mentha, belonging to the Lamiaceae family, is a genus of aromatic plants renowned for its medicinal, culinary, and therapeutic importance (Anwar et al. 2019). *M. royleana* is one of the important traditionally used medicinal plants. It belongs to this genus (Phatak and Heble 2002). *M. royleana* can be found in various parts of Pakistan (Chitral, Hazara, Kashmir and Swat), South Africa, India, Nepal and Europe. This plant is used traditionally for gastrointestinal disturbances like gas trouble, indigestion, vomiting and cholera (Khan et al. 2011). The current study was aimed to evaluate metabolites of the *M. royleana* via GC-MS and to evaluate the anti-spasmodic, anti-ulcer and anti-diarrheal potentials of various solvents based fractions to provide scientific base for the traditional uses of the plant in gastrointestinal disorders.

The two important genes CHRM3 and CACNA1C regulate the GIT motility at molecular level through encoding the M3 muscarinic receptor and L-type voltage-gated calcium channel (Cav1.2) respectively (Feng et al. 2024). Collectively these proteins are crucial for intracellular calcium signaling and contraction of smooth muscles. These proteins are important target for therapeutic involvementas dysregulation of these proteins and their molecular pathways result in hypermotility and gastrointestinal disorders(Zheng et al. 2025).Gastrointestinal motility is efficiently controlled by several molecular targets, among which the L-type voltage-gated calcium channels (Cav1.2) and M3 muscarinic acetylcholine receptor (M3R) play fundamental roles (Igarashi-Hisayoshi et al. 2023; Wegener et al. 2006). When activated, M3R protein results in increased intracellular calcium levels through cholinergic signaling and causes contraction of smooth muscles (Ambudkar 2009).Likewise, calcium influx into smooth muscles is controlled by Cav1.2 and thus directly regulating muscle contraction and motility (Pereira et al. 2022).As deregulation of these pathways leads to spasmodic conditions, inhibition of Cav1.2 and M3R proteins is considered an important therapeutic approach for attaining antispasmodic effects and restoring normal GIT function.

The phytochemical profile of *M. royleana* was previously investigated using GCMS analysis, resulting in the identification of several important biologically active compounds. The presence of these compounds suggests a significant chemical basis for recognizing the biological activities of the plant. However, purification and experimental evaluation of all recognized phytochemicals is time consuming and resource intensive process. Therefore, the computational approach designed for the study provides an efficient alternative for screening and prioritizing compounds based on their potential bioactivity, safety, and molecular interactions with corresponding protein targets.

In this perspective, the current study is designed as a purely in silico exploration to estimate the therapeutic potential of GCMS identified compounds of *Mentha royleana* against important protein targets involved in GIT motility. The main aim of the study was to recognize potential lead candidates capable of targeting Cav1.2 and M3R proteins, thus contributing to the understanding of relevant molecular mechanisms linked with gastrointestinal motility and presenting a scientific basis for traditional use of *M. royleana*, along with supporting future experimental validation and drug development.

METHODOLOGY

GCMS analysis

The GC-MS analysis of crud extractwas performed by using Agilent USB-393752 system which was equipped with gas chromatograph and HHP-5MS capillary column (5%phenylmethylsiloxane) and mass selective detector working through electron impact mode. Compounds were identifiedby comparing the spectral data with those of NIST and Wiley libraries, secondly the fragmentation pattern was compared with previously published data.

QSAR prediction

Many compounds were identified by GCMS out of which 20 compounds, were computationally studied for their structure-activity relationship (SAR) i.e. effect on GIT motility. QSAR (Quantitative Structure Activity Relationship) analysis of the compounds was performed to predict their pIC50 against L-type voltage-gated calcium channel (Cav1.2) and M3 muscarinic acetylcholine receptor (M3R). To determine pIC50, experimental IC50 data was obtained from database ChEMBL (Gaulton et al. 2017) and used for training models. Machine learning algorithms including XGBoost, Gradient boosting, Support Vector Regression (SVR), and Random Forest were employed. The dataset was divided into 80% training and 20% testing sets for model development.

Safety and drug-likeness filters

For *in silico* analysis of the compounds, their SMILES were retrieved from online database PubChem(Kim et al. 2021). Using these SMILES, all 20 compounds were preliminary screened for drug-likeness characteristics by utilizing Lipinski, Veber, and PAINS filters. In the next step, the passed compounds were screened for safety by using toxicity prediction (TOX), Rapid Elimination of Swill (REOS), human Ether-à-go-go-Related Gene (hERG) filters.

Batch docking

To determine the binding affinity of all 20 selected compounds against selected target proteins, preliminary batch docking of the compounds was performed by Autodock Vina (Trott and Olson 2010). For batch docking, the 3D structures of the compounds (SDF files) were obtained from PubChem database, while the PDB files of target proteinsCav1.2(PDB IDs: 8FD7, 8WE8, 8WEA) and M3R(PDB IDs: 4DAJ, 4U14, 5ZHP)were retrieved from protein bank database RCSB (Burley et al. 2021).

Network pharmacology study

Network Pharmacology approach was used to elucidate the interaction between compounds and target proteins related to GIT motility. Potential targets Cav1.2 and M3R were identified based on batch docking analysis andendorsed by target prediction of compounds using platform swiss target prediction. The gene symbols CHRM3 of M3 muscarinic acetylcholine receptor and CACNA1C of L-type voltage-gated calcium channel were obtained from Uniport database (Ahmad et al. 2025). A compound–target interaction network was prepared using

Cytoscape (version 3.10.3), where different nodes indicated compounds and target proteins while edges represented interactions between compounds and their potential targets. To differentiate between interaction strengths, nodes are color-coded based on binding affinity values.

Selection of best ligands

The five best compounds were selected for further detailed study, using parameters like preliminary binding affinity obtained from batch docking, drug-likeness analysis, safety filters, and predicted pIC50. The selected compounds were further subjected to detailed molecular docking study, drug-likeness characteristics, ADMET analysis and density functional theory (DFT) analysis.

Density functional theory (DFT) analysis

The selected top five selected ligands were subjected to density functional theory analysis to evaluate their structure stability and electronic properties. The 3D structures (SDF format) of ligands were initially optimized by Avogadro (version 1.9) using forcefield MMFF94 to obtain satisfactory starting configurations. After preliminary geometry optimization, ligands were saved as XYZ format. To perform DFT analysis of the compounds, ORCAsoftware (6.1) was employed (Neese 2025).Full geometry optimization was performed using the B3LYP exchange–correlation functional in combination with the 6-31G(d) basis set, under tight self-consistent field (TightSCF) convergence criteria, to obtain energetically stable structures. After DFT analysis, important quantum chemical parameters like Dipole moment, highest occupied molecular orbital (HOMO), and lowest unoccupied molecular orbital (LUMO) energies were extracted from output files. In addition, optimized ligands (XYZ format) were converted back to SDF and subsequently to PDB format by Avogadro and Openbabel respectively to be used further in molecular docking study.

Ligand preparation

DFT optimized ligands were protonated at physiological pH, using Open Babel (O'Boyle et al. 2011), to ensure proper ionization states required for functioning of target proteins. The ligands were subsequently processed in Autodock Tools (version 1.5.7) by addition of polar hydrogen, assigning rotatable bonds andcomputing Gasteiger charges (Morris et al. 2009). Finally, the ligands were saved in PDBQT format for docking.

Target preparation

Two target proteins Cav1.2(PDB ID: 8WE8) and M3R(PDB ID: 5ZHP)were selected for detailed molecular docking study. PDB structure8WE8correspondsto human L-type voltage-gated calcium channel (Cav1.2) having resolution of 2.90 Å(Gao et al. 2023) and co-crystallized inhibitor while 5ZHPrepresents*Rattus norvegicus*M3 muscarinic acetylcholine receptor (M3R) having resolution of 3.10 Åand co-crystalized inhibitor (Liu et al. 2018). The PDB structures of the proteins were cleaned in Discovery Studio(Biovia 2017) by removing unnecessary components like co-crystallized ligands, cofactors, ions and water molecules while retaining important ones where required. The cleaned 3D structures were then converted to PDBQT format after addition of hydrogen and Kollman charges in Autodock tools. The grid box dimensions for docking were defined based on binding sites of co-crystallized ligands. For Cav1.2 (8WE8), the grid box center was set at (x = 150, y = 168, z = 152) with dimensions of (x = 25, y = 35, z = 25). For M3R (5ZHP), the grid box center was set at (x = −23, y = −48, z = 197) with dimensions of (x = 28, y = 28, z = 28).

Validation of docking protocol

The docking protocol was validatedby redocking co-crystallized into their respective binding sites. The root mean square deviation (RMSD) between the experimental and predicted poses was determined. The co-crystallized ligands tiotropium in 5ZHP and amlodipine in 8WE8 were extracted from proteins and exported as PDB format using software Discovery studio. Both ligands were then protonated at pH 7.4 using Open Babel, prepared for docking in Autodock tools by adding polar hydrogen, assigning rotatable bonds and computing Gasteiger charges and converted to PDBQT format. The prepared ligands were redocked against respective proteins by Autodock Vina to determine the binding affinity and RMSD was calculated in PyMOL (2.5.4 version) (Schrodinger 2015).

Molecular docking study

A detailed docking study of the five selected compounds against target proteins Cav1.2(PDB ID: 8WE8) and M3R(PDB ID: 5ZHP)were performed using Autodock Vina, Discovery Studio and PyMOL. The binding affinity of each ligand–protein complexwas determined in terms of binding energy(kcal/mol). The docking pose with lowest binding energy was selected as most favorable confirmation. The predicted binding site was validated by comparing with binding site of respective co-crystallized ligands. The docked complexeswere visualized by Discovery Studio to study key contact residues and visualize ligand–protein interactions in 2D format. Furthermore, PyMOL (DeLano 2002) was used for 3D visualization and calculating hydrogen and hydrophobic bond lengths (angstrom) within the complexes.

In silico pharmacokinetics and toxicity analysis

An online webtool pkCSM is used to predict the pharmacokinetic properties (absorption, distribution, metabolism, excretion) and toxicity profiles of compounds (Pires et al., 2015).The SMILES of selected compounds were submitted to pkCSM server to evaluate key ADMET parameters likehuman intestinal absorption, Caco-2 permeability, P-glycoprotein (P-gp) substrate and inhibitor potential, volume of distribution (VDds), blood–brain barrier permeation, CYP2D6 inhibitor, CYP3A4 inhibitor, total clearance, AMES mutagenicity, hERG inhibition (cardiotoxicity), hepatotoxicity, LD50 / acute toxicity (rat), and skin sensitization.

Drug-likeness study

Drug-likeness properties of the selected compounds were predicted by SwissADME webserver to evaluate their suitability as orally active drug candidates (Daina et al., 2017). The SMILES of the compounds were submitted to SwissADME for analysis. Lipinski's Rule of Five was used to study oral bioavailability related properties like molecular weight, lipophilicity, hydrogen bonds donors and acceptors. Veber's rule also evaluated oral bioavailability based on topological polar surface area (TPSA). Additionally, Ghose filter was used to study molecular weight, logP, molar refractivity, and total number of atoms of the compounds. Compounds' synthetic accessibility was evaluated to predict their ease of chemical synthesis. PAINS (Pan-Assay Interference Compounds) and Brenk filters to predict potentially problematic substructures that may result in false-positive bioactivity or toxicity.

RESULTS

GCMS Analysis

Multiple compounds were identified in *Metha royleana* plant extract through GCMS analysis. Table for identified compounds are given below,

Table 1. List of compounds identified in *M. royleana* crude methanolic extract

S.No.	Compound Name	Formula	Mol. wt
1.	1-Butanol, 3-methyl	$C_5H_{12}O$	*88.1482*
2.	Propanamide, 2-methyl	C_4H_9NO	87.1204
3.	Guanidine, N,N-dimethyl	$C_3H_9N_3$	87.1237
4.	N,N-Dimethylacetamide	C_3H_7NO	*73.09*
5.	Toluene	C_7H_8	92.14
6.	Acetamide, 2,2,2-trifluoro-	*$C_2H_2F_3NO$*	113.0386
7.	4-Fluorohistamine	$C_5H_8FN_3$	*129.1355*
8.	1-Methyldecylamine	$C_{11}H_{25}N$	*171.3229*
9.	Phenethylamine, p,.alpha.-dimethyl-	$C_{10}H_{15}N$	149.2328
10.	1-Octadecanamine, N-methyl-	$C_{19}H_{41}N$	283.5355
11.	1-Propanol, 2-amino	*C_3H_9NO*	75.11
12.	Vanillin	$C_8H_8O_3$	152.15
13.	Benzaldehyde, 3-hydroxy-4-methoxy-	$C_8H_8O_3$	152.1473
14.	Methylpent-4-enylamine	$C_6H_{11}N$	97.16
15.	Pentanal	$C_5H_{10}O$	86.13
16.	3,3-Dimethyl-4-methylamino-butan-2-one	$C_{10}H_20N_2O$	168.2
17.	Propanamide	C_3H_7NO	59.09
18.	Cyclobutanol	C_4H_8O	72.11
19.	Paradrine	$C_{10}H_{11}NO_2$	163.20
20.	Glutaraldehyde	$C_5H_8O_2$	100.12
21.	Benzeneethanamine, N-methyl-	$C_8H_{10}N$	122.17
22.	Butylated Hydroxytoluene	$C_{20}H_{28}O2$	308.44
23.	Butanal	C_4H_8O	72.11
24.	3-Cyclohexyl-1-methyl-1-(2-phenylethyl)urea	$C_{20}H_{23}N_3O$	
25.	n-Butylethylenediamine	$C_6H_{14}N_2$	102.19

26.	Alanylglycine, TMS	$C_6H_{11}NO_4$	129.16
27.	Diethyl Phthalate	$C_{10}H_{12}O_4$	222.20
28.	Benzoic acid, 2-(1-oxopropyl)-	$C_{11}H_{12}O_4$	192.21
29.	Norephedrine	$C_{10}H_{13}NO$	165.22
30.	3-(2-Aminopropyl)phenol	$C_{11}H_{15}NO$	177.25
31.	1-[.alpha.-(1-Adamantyl)benzylidene]thiosemicarbazide	$C_{20}H_{25}N_3S$	229.50
32.	2-Amino-1-(o-hydroxyphenyl)propane	$C_{11}H_{16}N_2O_2$	192.26
33.	Atomoxetine	$C_{10}H_{11}NO$	179.20
34.	2-Hexanamine, 5-methyl	$C_7H_{18}N$	114.23
35.	Acetamide, 2-cyano	$C_5H_7NO_2$	97.12

QSAR analysis

Machine learning models including XGBoost, Gradient boosting, Support Vector Regression (SVR), and Random Forest were analyzed by performance metrics such as coefficient of determination (R^2), mean absolute error (MAE), and root mean square error (RMSE) to determine the best performing model. Among these, XGBoost was found to be best performance model as shown by its highestR^2 along with the lowest MAE and RMSE values as shown in Figure 1. Subsequently, XG boost was used to predict the pIC50 of all selected 20 compounds against Cav1.2 and M3R as shown in Table 2. Among the evaluated compounds,Atomoxetine, 3-Cyclohexyl-1-methyl-1-(2-phenylethyl)urea and 1-[alpha-(1-Adamantyl)benzylidene]thiosemicarbazidehas shown highest pIC50 against target proteins. Especially, Atomoxetine demonstrated highest pIC50 of 6.11 against target M3R, suggesting stronger inhibitory potential. Overall, predicted pIC50 values (3.91-6.11) exhibited moderate activity of compounds against selected targets.

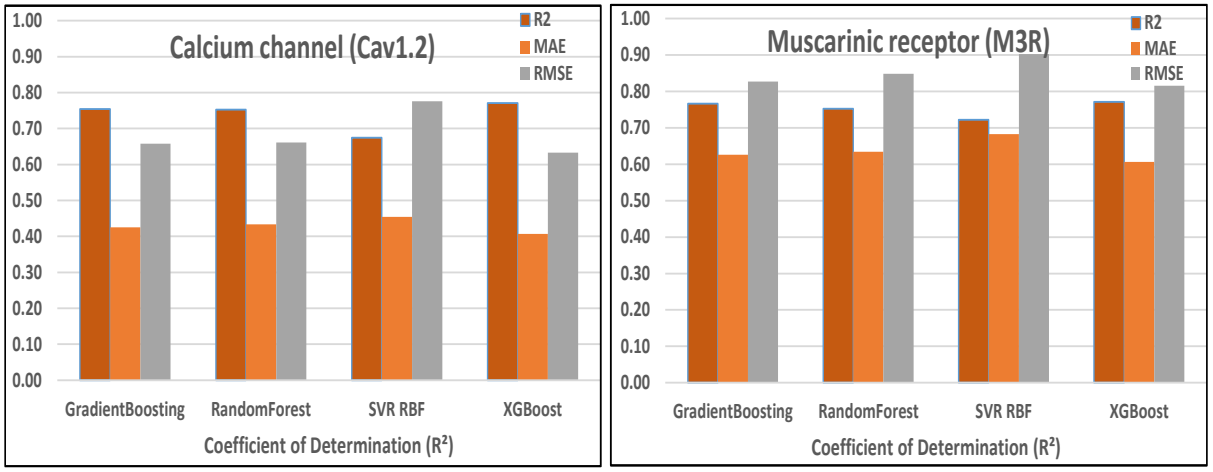

Figure 1. Performance metrics Coefficient of determination (R^2), Mean Absolute Error (MAE), and Root Mean Square Error (RMSE) of ML-models

Table 2. Predicted inhibitory activity (pIC50) of compounds against selected targets by best performance ML-model XGBoost

Compound ID	CompoundName	pIC50 against Cav1.2	pIC50 against M3R
CPD1	1-[alpha-(1-Adamantyl)benzylidene]thiosemicarbazide	4.85	5.51
CPD2	1-Methyldecylamine	4.04	5.65
CPD3	2-Amino-1-(o-hydroxyphenyl)propane	3.91	5.04
CPD4	2-Hexanamine, 5-methyl	3.79	5.61
CPD5	3-(2-Aminopropyl)phenol	3.94	4.73
CPD6	3,3-Dimethyl-4-methylamino-butan-2-one	3.68	4.81
CPD7	3-Cyclohexyl-1-methyl-1-(2-phenylethyl)urea	4.92	5.67
CPD8	4-Fluorohistamine	3.71	5.69

CPD9	Atomoxetine	4.85	6.11
CPD10	Benzaldehyde, 3-hydroxy-4-methoxy	3.31	5.15
CPD11	Benzeneethanamine, N-methyl	3.98	5.39
CPD12	Butylated Hydroxytoluene	4.84	5.22
CPD13	Diethyl Phthalate	4.71	5.11
CPD14	Glutaraldehyde	3.85	5.16
CPD15	Methylpent-4-enylamine	4.23	4.99
CPD16	n-Butylethylenediamine	3.81	5.15
CPD17	Norephedrine	3.78	5.36
CPD18	Paradrine	4.02	4.76
CPD19	Phenethylamine, p,alpha-dimethyl	3.92	5.50
CPD20	Vanillin	3.33	5.04

Preliminary drug-likeness, safety and binding affinity analysis

All 20 compounds were subjected to preliminary drug-likeness and safety analysis along with batch docking. Batch docking exhibited binding affinities of compounds against target structures Cav1.2 (PDB IDs: 8FD7, 8WE8, 8WEA) and M3R (PDB IDs: 4DAJ, 4U14, 5ZHP) in the range of -3.5 to -10 kcal/mol as shown in Figure 2. The heatmap representation indicates variation in binding affinities where green color shows stronger interaction while red color shows weaker interaction. Especially,compound CPD1 has shown strong affinity against targets M3Rwith binding affinity -9.6 kcal/mol. Similarly, CPD7 has demonstrated strong binding affinity against (-8.5 kcal/mol) against M3R as shown in Table 3. Additionally, CPD9 has also demonstrated comparatively stronginteraction with targets as evident from binding affinity against target proteins.However, despite good binding affinity scores, some compounds like CPD7, CPD9, and CPD12 did not pass preliminary safety filters. Overall, most of the compounds have good interactions with target proteins and qualified drug-likeness and safety analysis.

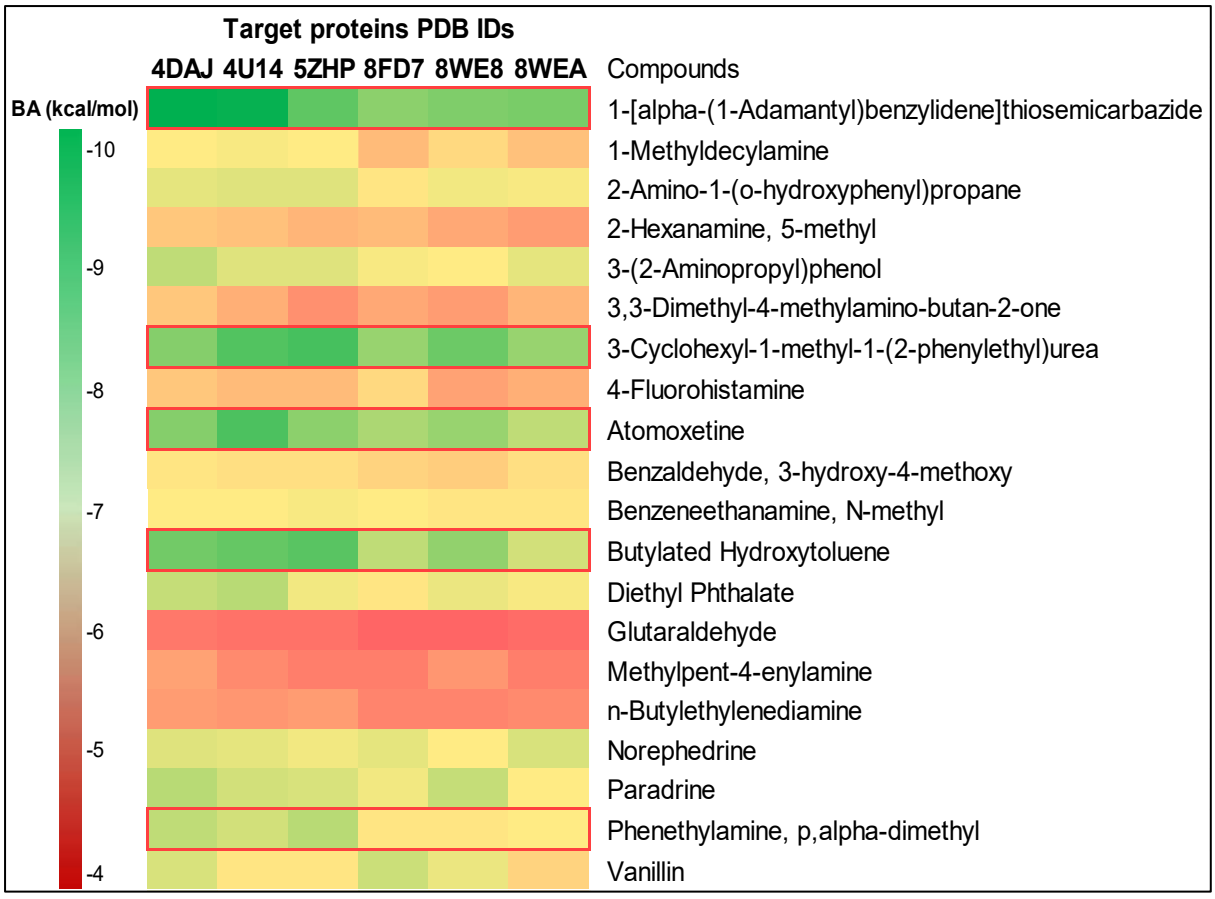

Figure 2. Heatmap demonstration of binding affinities (kcal/mol) of compounds against targetproteins. Color variation from green to red represents strong to weak binding affinity

Table 3. Preliminary binding affinity, drug-likeness and safety analysis of compounds (CPD1-CPD20)

Compound	Binding affinity (kcal/mol)						Drug-likeness filter	Safety filter
	Cav1.2			M3R				
	8FD7	8WE8	8WEA	4DAJ	4U14	5ZHP		
CPD1	-7.4	-7.6	-7.7	-9.6	-9.5	-8.1	Pass	Pass
CPD2	-4.8	-5.3	-4.9	-5.6	-5.7	-5.6	Pass	Pass
CPD3	-5.5	-5.8	-5.7	-6.0	-6.1	-6.1	Pass	Fail
CPD4	-4.8	-4.5	-4.3	-5.0	-4.9	-4.7	Pass	Pass
CPD5	-5.7	-5.6	-6.0	-6.6	-6.1	-6.1	Pass	Fail
CPD6	-4.5	-4.3	-4.7	-5.0	-4.6	-4.1	Pass	Pass
CPD7	-7.2	-7.9	-7.2	-7.5	-8.3	-8.5	Pass	Fail
CPD8	-5.3	-4.4	-4.6	-5.0	-4.8	-4.8	Pass	Pass
CPD9	-6.9	-7.2	-6.6	-7.5	-8.4	-7.4	Pass	Fail
CPD10	-5.2	-5.1	-5.4	-5.5	-5.4	-5.4	Pass	Fail
CPD11	-5.6	-5.5	-5.5	-5.6	-5.6	-5.7	Pass	Pass
CPD12	-6.6	-7.3	-6.3	-7.8	-8.0	-8.2	Pass	Fail
CPD13	-5.5	-5.9	-5.7	-6.5	-6.7	-5.8	Pass	Pass
CPD14	-3.4	-3.4	-3.5	-3.7	-3.6	-3.6	Pass	Pass
CPD15	-3.8	-4.2	-3.8	-4.4	-4.0	-3.8	Pass	Pass
CPD16	-3.9	-3.9	-4.0	-4.3	-4.2	-4.3	Pass	Pass
CPD17	-6.0	-5.6	-6.2	-6.1	-6.0	-5.8	Pass	Pass
CPD18	-5.8	-6.5	-5.6	-6.7	-6.3	-6.2	Pass	Fail
CPD19	-5.5	-5.5	-5.6	-6.6	-6.3	-6.7	Pass	Pass
CPD20	-6.4	-5.9	-5.2	-6.2	-5.5	-5.5	Pass	Fail

Network pharmacology

Network pharmacology analysis demonstrated the visualization of interactions between compounds andgastrointestinal-motilityrelated proteins using Cytoscape. The strength of interactions between compounds and their targets were shown by different colors of nodes and edges as illustrated in Figure 3. Compounds such as 1-[alpha-(1-Adamantyl)benzylidene]thiosemicarbazide, 3-Cyclohexyl-1-methyl-1-(2-phenylethyl)urea, Atomoxetine, and Butylated Hydroxytolueneoccupied central positions in the network linking to both targets CHRM3 (M3R) and CACNA1C (Cav1.2). Target prediction by swisstargetprediction supported few important docking interactions of compounds against CHRM3 (M3R).The dual interaction of these compounds with targets predicted their potential role in modulating GIT motilityvia mutual antispasmodic activity and calcium channel blockade mechanisms.

Based on results of pIC50 prediction, preliminary drug-likeness andsafety screening, and binding affinity analysis of all selected 20 compounds against multiple target structuresof target proteins (Cav1.2 and M3R), five compounds were selected for further analysis. These included compounds 1-[alpha-(1-Adamantyl)benzylidene]thiosemicarbazide (CPD1), 3-Cyclohexyl-1-methyl-1-(2-phenylethyl)urea (CPD7), Atomoxetine (CPD9), Benzeneethanamine(CPD11), and N-methyl, Phenethylamine, p,alpha-dimethyl (CPD19).The selected compounds exhibited comparatively higher pIC50, lowest binding affinity and passing druglikness and safety filters. Although CPD7 and CPD9 could not pass initial safety filters,they were keptbecause of their superior binding affinity and predicted biological activity demanding detailed investigation. For subsequent detailed docking study,two representative PDB structures 8WE8 and 5ZHP were selected because of comparatively high resolution and presence of co-crystallized inhibitor.

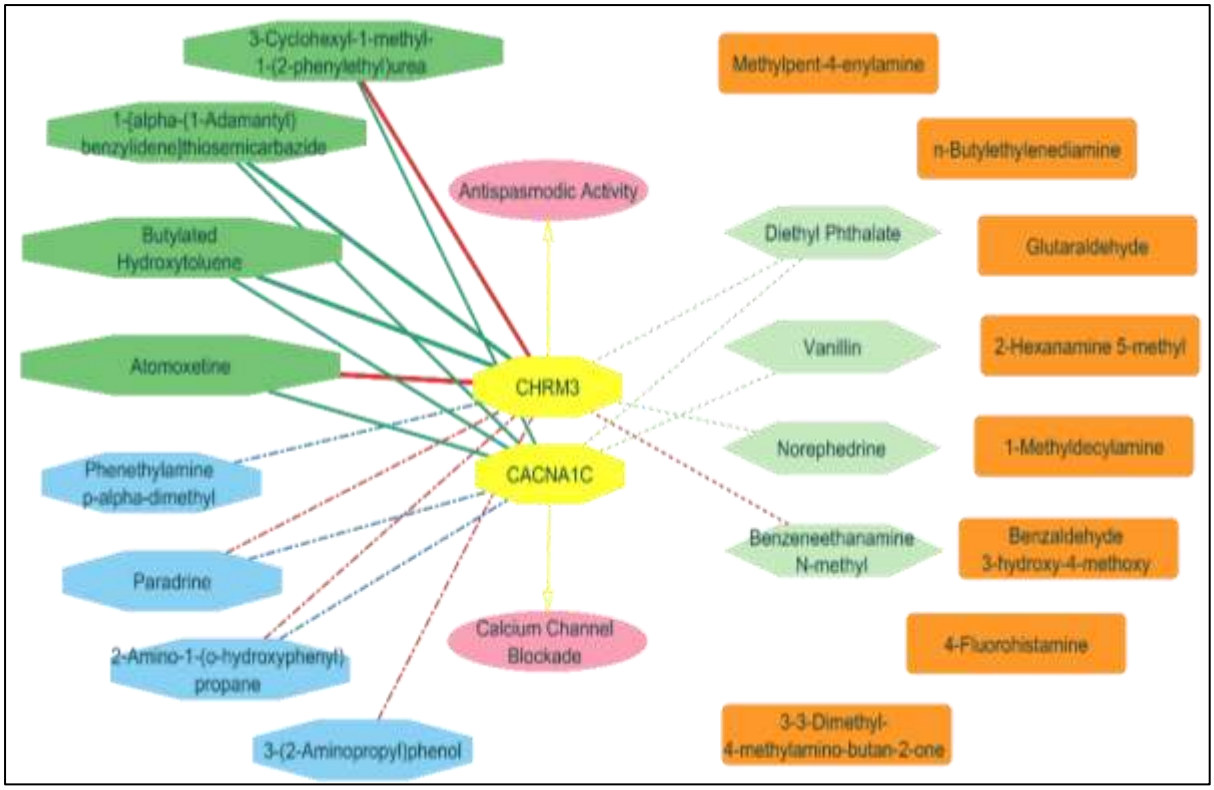

Figure 3. Network pharmacology representation of compounds with targets. Compounds and targets are shown in nodes, while edges represent interactions between them. Dark green nodes indicate strong interactions.Blue nodes represent moderate interactions. Light green nodes represent weak interactions. Orange nodes with no edges represent very weak or no interactions. Red color edges represent interactions supported by both docking and swisstargetprediction.

Density functional theory (DFT) analysis

DFT analysis calculated HOMO and LUMO energies, dipole moment, and total electronic energy of selected compounds as shown in Table 4. The compounds LUMO energies were found to be in the range of -0.598 to 0.204 eV, whereas HOMO energies ranged from -6.063 to -5.317 eV. HOMO-LUMO gap (ΔE) was found to be lowest for CPD1 (4.719 eV) and highest for CPD19 (6.268 eV). Molecular polarity was determined by measuring dipole moment of 3D structures of compounds which was obtained as 0.927 to 5.943 Debye. Total electronic energy was highest for CPD11 (-405.250Hartree) and lowest for CPD1 (-1261.580Hartree).

Table 4. DFT-calculated quantum chemical parameters of the selected compounds at optimized geometry

Ligands	E_{LUMO} (eV)	E_{HOMO} (eV)	ΔE (eV)	Dipole moment (D)	Total energy (Hartree)
CPD1	-0.598	-5.317	4.719	5.943	-1261.580
CPD7	-0.079	-5.972	5.893	3.534	-808.383
CPD9	-0.087	-5.604	5.518	1.548	-789.899
CPD11	0.203	-5.830	6.032	0.927	-405.250
CPD19	0.204	-6.063	6.268	1.342	-444.545

Docking validation

Root mean square deviation (RMSD) was calculated as less than 2.0 Å by redocking co-crystallized ligands against respective protein structures as shown in Figure 4. The co-crystallized tiotropium was redocked into M3R(5ZHP) and RMSD was found to be 0.835Åbetween the crystallographic pose and best docked pose with binding affinity -11.2 kcal/mol.Similarly, RMSD of 0.932 Å was calculated by redocking amlodipine against Cav1.2 (8WE8) and binding affinity was found to be -6.9 kcal/mol. These results verify the reliability of the docking protocol.

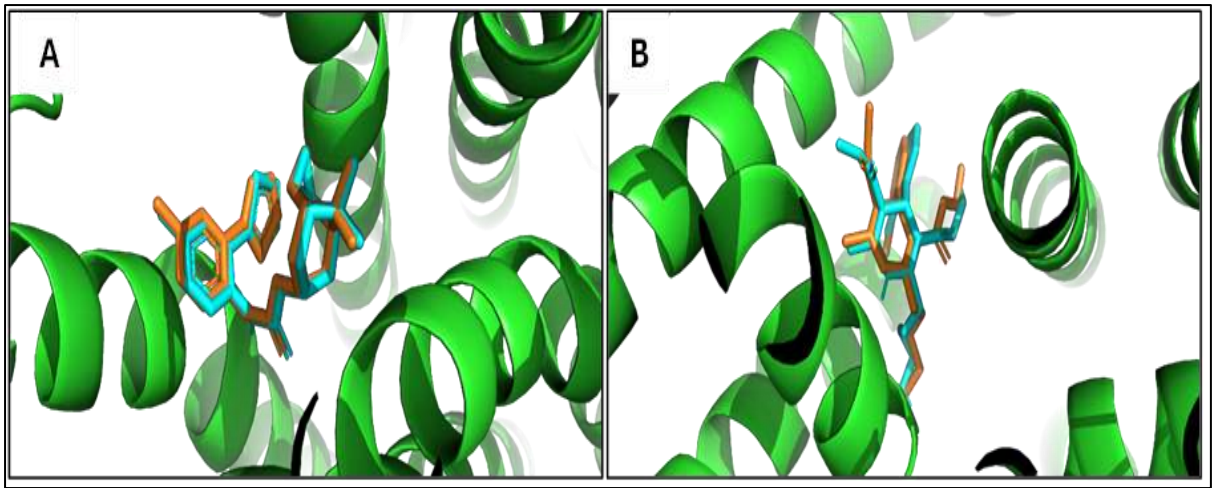

Figure 4. RMSD measurement betweenexperimental and redocked poses against respective proteins.(A) Superimposition of the crystallographic and docked poses of tiotropiumin M3R (PDB ID: 5ZHP)indicating an RMSD of 0.835 Å. (B) Superimposition of amlodipine in Cav1.2 (PDB ID: 8WE8) exhibiting and RMSD of 0.932 Å.

Molecular docking analysis

Detailed molecular docking analysis determined the binding affinity, interacting residues, interaction types, and bond lengths between selected ligands and binding site of target proteins as summzarized in Table 5. After docking, the best binding pose of each ligand was selected on basis of lowest binding energy andfurther validated bycomparing it with binding site of experimental inhibitor ligand to ensure the correct binding site and inhibitory potential of compounds against target proteins as shown in Figure 5. The interacting residues at binding site of the ligands were visualized in 2D with Discovery studio while 3D visualization was done in PyMOL as shown in Figure 6 and 7 respectively. Among the evaluated compounds, Compound CPD1 has shown strongest interaction with both targets having binding affinity of -9.7 and -8.6 kcal/mol against M3R (5ZHP) and Cav1.2 (8WE8) respectively.In Cav1.2, CPD1 formed a hydrogen bond withMET1509 having length of 3.0 Å as shown in Figure 7B, while hydrophobic interactions with residues ILE1049, VAL1053, PHE1181, and PHE1513 ranged from 2.6 to 3.6 Å. Similarly, CPD1 also formed hydrophobic bonds with residues TYR148, ALA238, TRP503, and TYR529 at binding site of M3R with bond lengths ranging from 2.4 to 3.4 Å (Figure 7A). The compound CPD7has also shown strong interaction with M3R with binding affinity -8.3 kcal/mol, which was evident from strong hydrogen bond (2.0 Å) with residue TYR506 (Figure 7C). Similarly, compounds CPD11 and CPD19 have also formed hydrogen bonds with TYR529 and MET1509 of M3R and Cav1.2 proteins at binding site with bonds length 2.3 and 1.9 Å respectively.

Table 5: Binding affinity (kcal/mol), interacting residues, hydrogen and hydrophobic interactionsof studied compounds with target proteins

Ligand	Target protein	PDB ID	Binding affinity (kcal/mol)	Hydrogen interactions	Hydrophobic interactions	Bonds length (Å)
CPD1	*L-type voltage-gated calcium channel (Cav1.2)	8WE8	-8.6	MET1509	ILE1049 VAL1053 PHE1181 PHE1513	2.6-3.6
	**M3 muscarinic acetylcholine receptor (M3R)	5ZHP	-9.7	---	TYR148 ALA238 TRP503 TYR529	2.4-3.4
CPD7	L-type voltage-gated calcium channel (Cav1.2)	8WE8	-7.8	---	VAL1053 PHE1181 MET1178	3.2-3.4
	M3 muscarinic acetylcholine receptor (M3R)	5ZHP	-8.3	TYR506	ALA238 TYR529	2.0-3.3
CPD9	L-type voltage-gated calcium channel (Cav1.2)	8WE8	-7.5	---	ILE1046 VAL1053 PHE1181 PHE1513	3.0-3.8

	M3 muscarinic acetylcholine receptor (M3R)	5ZHP	-8.3	---	TYR148 TRP199 ALA238 TRP503 TYR506 TYR529	2.5 – 4.0
CPD11	L-type voltage-gated calcium channel (Cav1.2)	8WE8	-5.4	---	VAL1053 PHE1181	2.8-3.5
	M3 muscarinic acetylcholine receptor (M3R)	5ZHP	-5.7	TYR529	TRP503	2.3-3.5
CPD19	L-type voltage-gated calcium channel (Cav1.2)	8WE8	-5.8	MET1509	ILE1049 PHE1181 PHE1513	1.9-3.4
	M3 muscarinic acetylcholine receptor (M3R)	5ZHP	-6.4	---	TYR506 TYR529 CYS532	3.3-3.9

*L-type voltage-gated calcium channel (Cav1.2) is derived from *Homo sapiens* (PDB ID: 8WE8).
**M3 muscarinic acetylcholine receptor (M3R) is derived from *Rattus norvegicus* (PDB ID: 5ZHP).

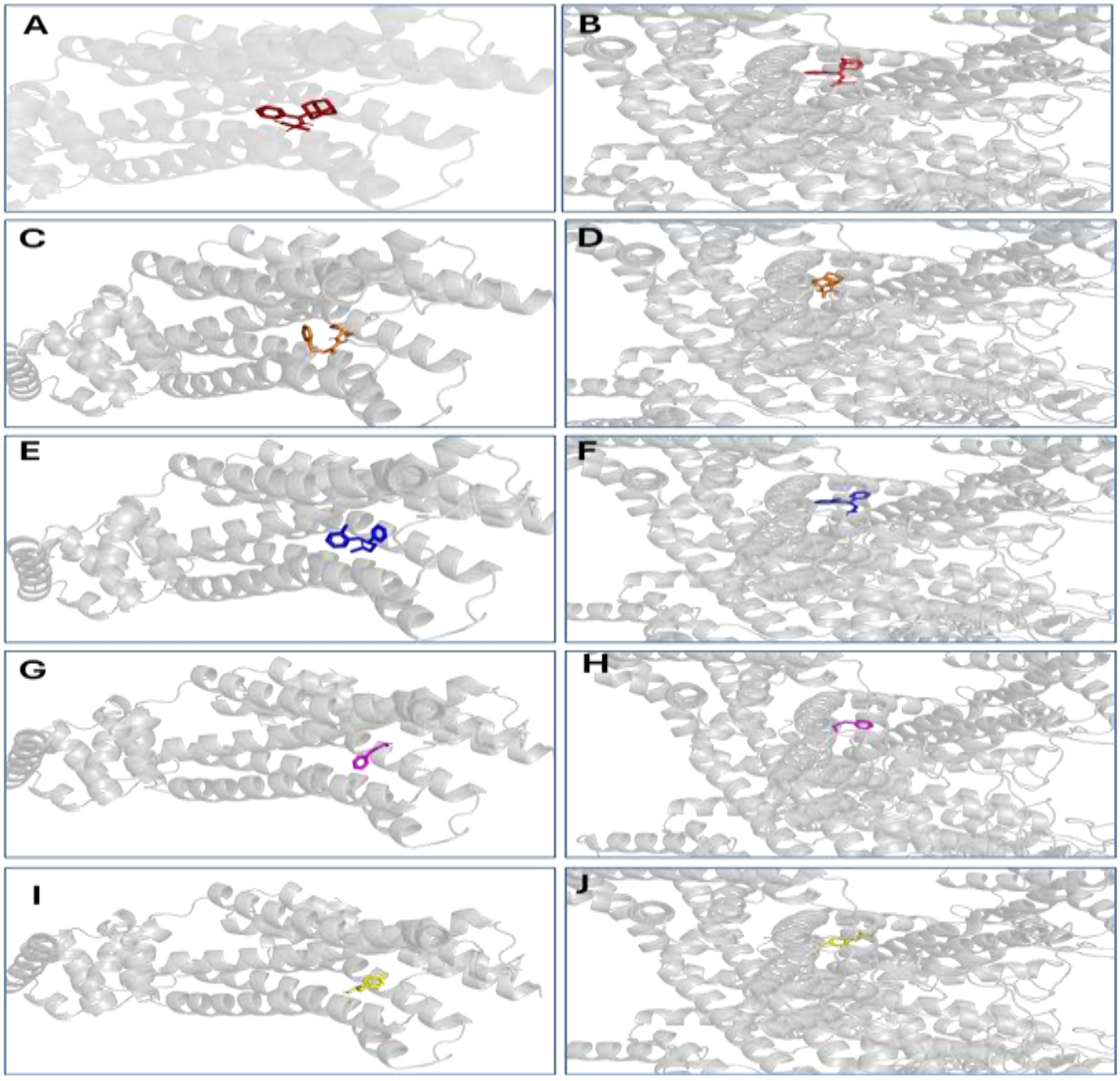

Figure 5: Molecular docking confirmations of selected compounds against target proteins. (A,C,E,G,I) Best binding confirmation of CPD1, CPD7, CPD9, CPD11, and CPD19 with M3R. (B,D,F,H,J) Best binding confirmation of CPD1, CPD7, CPD9, CPD11, and CPD19 with Cav1.2. Gray colored ribbons represent protein structures, while colored sticks represent docked ligands at best binding orientation.

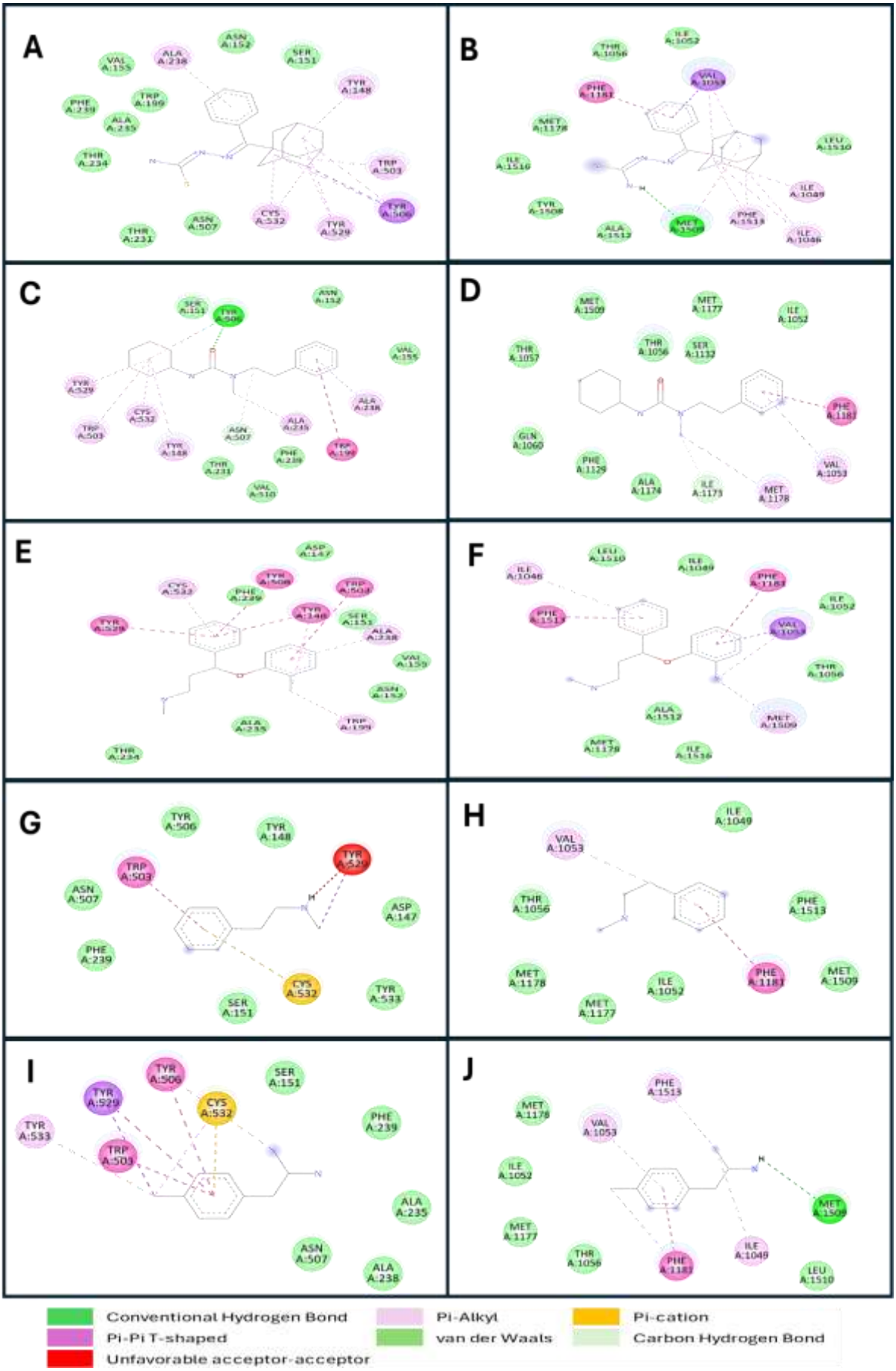

Figure 6: Two-dimensional (2D) visualization of docking interactions of selected ligands with targets in Discovery Studio. (A,C,E,G,I) Interactions of CPD1, CPD7, CPD9, CPD11, and CPD19 with M3R. (B,D,F,H,J) Interactions of CPD1, CPD7, CPD9, CPD11, and CPD19 with Cav1.2. Dotted green lines show hydrogen interactions while dotted pink lines show hydrophobic interactions.

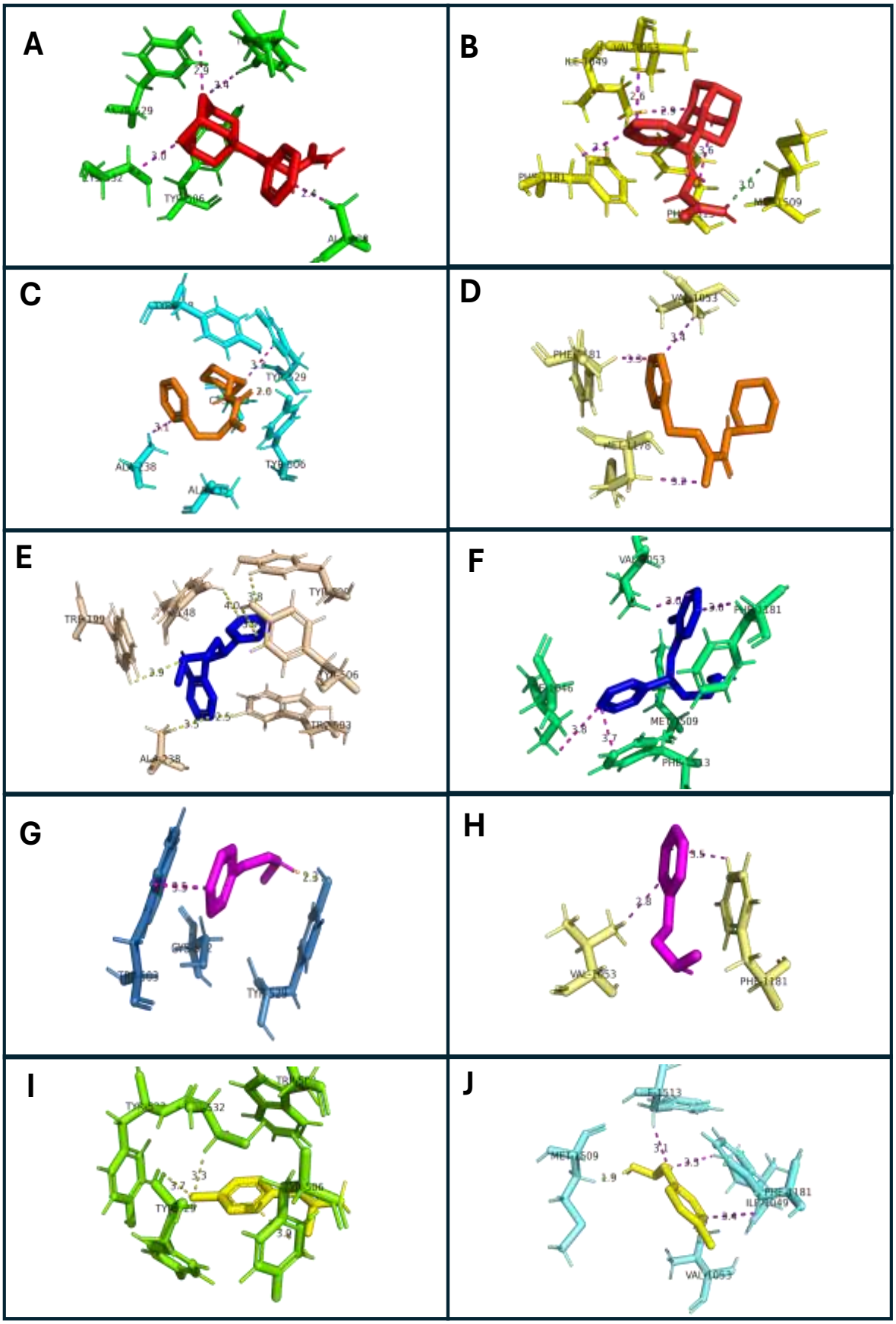

Figure 7. Three-dimensional (3D) visualization of docking interactions of selected ligands with targets in PyMOL. (A,C,E,G,I) Interactions and bonds length of CPD1, CPD7, CPD9, CPD11, and CPD19 with M3R. (B,D,F,H,J) Interactions and bonds length of CPD1, CPD7, CPD9, CPD11, and CPD19 with Cav1.2.

In silico pharmacokinetics and toxicity

The ADMET profiles of compounds CPD1, CPD7, CPD9, CPD11, and CPD19 were predicted using pkCSM server and results are summarized in Table 6. The predicted human intestinal absorption of all compounds was found to be high, ranging from 91.6 to 94.9 %, suggesting good oral bioavailability, which was further supported by Caco-2 permeability values (log Papp: 1.36–1.73) indicating favorable membrane permeability. Among the compounds, only CPD9 was found to act as both inhibitor and substrate of p-glycoprotein, while CPD1 was found to act as substrate only. Other compounds did not show any interaction with p-glycoprotein. The volume of distribution (VDss) of selected compounds was predicted in the range of 0.442 to 1.725 log L/kg, with CPD9 showing highest value (1.725 log L/kg). Blood brain barrier (BBB) permeability was found to be lowest for CPD1 (-0.149 log BB) while highest for CPD9 0.741 log BB. All the compounds were predicted to be non-inhibitors of CYP2D6 and CYP3A4, except CPD9 and CPD19 which were found to inhibit CYP2D6 enzyme suggesting metabolic interactions. Compound CPD7 was predicted to have faster elimination as suggested by its highest total clearance value (1.237 log ml/min/kg). All the studied compounds were found to be non-mutagenic and non-cardiotoxic except CPD9 which was predicted to be mutagenic. However, hepatotoxicity was predicted for CPD1, CPD9, and CPD19.Acute toxicity (LD_{50}) values of compounds suggested moderate toxicity levels. Skin sensitization was predicted for compounds CPD11 and CPD19, while the other compounds were found to be non-sensitizers.

Table 6. Pharmacokinetic and toxicity profiles of compounds obtained from pkCSM.

Category	Key Property	CPD1	CPD7	CPD9	CPD11	CPD19	Units
Absorption	Human Intestinal Absorption	91.673	91.98	93.774	94.95	91.7	%
	Caco-2 permeability	1.368	1.61	1.725	1.511	1.475	log Papp
	P-gp inhibitor	No	No	Yes	No	No	Yes/No
	P-gp substrate	Yes	No	Yes	No	No	Yes/No
Distribution	Volume of Distribution (VDss)	0.486	0.442	1.725	0.838	1.108	log L/kg
	Blood–Brain Barrier permeation	-0.149	0.305	0.741	0.246	0.411	log BB
Metabolism	CYP2D6 inhibitor	No	No	Yes	No	Yes	Yes/No
	CYP3A4 inhibitor	No	No	No	No	No	Yes/No
Excretion	Total clearance	-0.559	1.237	0.865	1.033	0.832	log ml/min/kg
Toxicity	AMES mutagenicity	No	No	Yes	No	No	Yes/No
	hERG inhibition (cardiotoxicity)	No	No	No	No	No	Yes/No
	Hepatotoxicity	Yes	No	Yes	No	Yes	Yes/No
	LD50 / acute toxicity (rat)	2.965	2.51	2.656	2.422	2.452	mol/kg
	Skin sensitization	No	No	No	Yes	Yes	Yes/No

Drug-likeness prediction of compounds

SwissAMDE platform was used to predict drug-likeness characteristics of the compounds CPD1, CPD7, CPD9, CPD11, and CPD19 as shown in Table 7. All the five compounds passed Lipinski's Rule of Five and Veber's rule, suggesting promising physicochemical properties required for oral absorption. Compounds CPD1, CPD7, and CPD9complied with the Ghose criteria while CPD11 and CPD19 did not fulfill Ghose requirements. The predicted bioavailability score of all the five compounds was found to be 0.55 suggesting moderate oral bioavailability. Synthetic accessibility score was found to be lowest for CPD11 (1.00), while highest (5.26) for compound CPD19 suggesting different levels of chemical synthesis of these compounds. Importantly, no PAINS alerts and Brenk alerts were found for all studied compounds except 2 structural alerts (imine and thiocarbonyl group)for CPD1.Overall, the compounds exhibited favorable drug-likeness profiles.

Table 7. Drug-likenessevaluationof selected compounds by SwissADME platform

Property	CPD1	CPD7	CPD9	CPD11	CPD19
Lipinski's Rule of Five	Yes	Yes	Yes	Yes	Yes
Veber's Rule (TPSA, RotB)	Yes	Yes	Yes	Yes	Yes
Ghose Filter	Yes	Yes	Yes	No	No
Bioavailability Score	0.55	0.55	0.55	0.55	0.55
Synthetic Accessibility Score	5.26	2.00	2.49	1.00	1.31

PAINS Filter	0 alert	0 alert	0 alert	0 alert	0 alert
Brenk Filter	2 alerts	0 alert	0 alert	0 alert	0 alert

DISCUSSION

The current study used an integrated computational approach including QSAR analysis, drug-likeness and safety filters, network pharmacology, DFT analysis and molecular docking study to evaluate bioactive metabolites identified by GC-MS analysis of *Mentha royleana*for their potential role in affecting GIT motility. This multi-step scheme resulted in effective prioritization of the study compounds by coupling structural properties with bioactivity, target engagement, and electronic features. By selecting two important protein targets, Cav1.2 and M3R, the study focused on mechanistically related framework for recognizing compounds with potential calcium channel blocking and antispasmodic activities. The merging of results obtained from different in silico techniques increases the reliability of the findings and supports the recognition of important lead candidates.

The QSAR approach was used to identify relationships between molecular structure of ligands and their biological activity by employing multiple machine learning algorithms (Soares et al. 2022; Patel et al. 2014). The best performing model XGBoost, based on metrics (high R2, low MAE and RMSE),suggested reliable early stage screening of the compounds and non-linear relationships between molecular descriptors and bioactivity. Although the pIC50 values predicted by XGBoost model were moderate, compounds CPD1, CPD7, and CPD9 haven shown relatively higher pIC50 values (4.85-6.11) against both targets Cav1.2 and M3R. The obtained pIC50 values still facilitated the prioritization of important compounds as very high potency is not always expected especially when source of compounds is natural or semisynthetic (Acosta et al. 2026; Lagunin et al. 2025).

The combination of drug-likeness criteria, toxicity screening, multi-target molecular docking, and network pharmacology delivers a thorough early stage filtering pipeline that augments the translational relevance of the results (Mou et al. 2025). The passing of initial Lipinski, Veber, PAINS filters by all compounds indicated promising physicochemical and pharmacokinetic properties of the compounds.The preliminary binding affinity (BA) screening helped in prioritizing compounds such as CPD1, CPD7, and CPD9 with BA values -7.2 to -9.6 kcal/mol against Cav1.2 and M3R, suggesting moderate to strong interaction with target proteins. Additionally, network pharmacology analysis supported most of these results by demonstrating that lead compounds can act on both CHRM3 (M3R) and CACNA1C (Cav1.2) targets simultaneously. This dual-target strategy is important for controlling smooth muscle contraction and calcium signaling at the same time, which is valuable in limiting GIT disorders (Feng et al. 2024). The identification of compounds demonstrating drug-likeness characteristics, strong binding affinities across multiple protein conformations, and acceptable safety profiles highlight their capability as lead compounds.

The selection of the five compounds was done on the basis of combined evaluation of QSAR analysis, docking results, drug-likeness features, safety profiles, and network pharmacology study, ensuring the prioritization process as authentic and balanced. Compounds CPD1, CPD7, CPD9, CPD11, and CPD19 were selected because of their steadily good performance across important criteria such as reasonable pIC50 values and good binding affinity against target proteins. Although compounds CPD7 and CPD9 failed the preliminary safety filter, they were still included in further analysis because of their strong binding interactions and higher predicted potency. This is a reasonable approach at initial stages of drug discovery where highly potent compounds are frequently retained for further study, as safety alarms can occasionally be addressed afterwards via structural variation and optimization (Kalgutkar 2011).

DFT analysis provides significant information about the electronic properties of compounds required to study ligand reactivity and stability (Hussain et al. 2025). Among the selected compounds, CPD1 exhibited lowest HOMO-LUMO energy gap (4.719 eV), demonstrating comparatively high chemical reactivity which was also evident from its strong binding interactions in preliminary docking analysis. In contrast, CPD19 has shown highest energy gap (6.268 eV) hinting greater stability but lower reactivity as demonstrated by its lower binding affinity values (-5.5 to -6.6 kcal/mol). The observed HOMO energies(−6.063 to −5.317 eV) of the compounds represented their ability to donate electrons required for interactions with target proteins. The dipole moment of CPD1 was found to be highest (5.943 D) indicating strong polarity and potential interaction within binding site of target proteins (Hagar et al. 2020). The total electronic energy calculations represent that all selected compounds attained stable optimized geometries, with CPD1 having the lowest energy, indicating its high structural stability. Overall, the DFT findings help the docking results by demonstrating that compounds like CPD1 possess a good balance of reactivity, polarity and stability.

The selection target proteins Cav1.2 and M3R were due to their well recognized and complementary roles in regulating GIT motility. Cav1.2 is required for smooth muscle contraction because it regulates the calcium influx in muscle cells while M3R protein facilitates cholinergic stimulation resulting in increased intracellular calcium and muscle contraction (Ghosh et al. 2025; Tanahashi et al. 2021). Inhibiting both the targets together provides a more comprehensive approach for attaining antispasmodic effect through modulating gastrointestinal motility (Igarashi-Hisayoshi et al. 2023; Wegener et al. 2006). The selection of two PDB structures 8WE8 (Cav1.2) and 5ZHP (M3R) were based on their relatively higher resolution, no missing atoms and residues, and presence of experimental inhibitors, which confirms proper identification of active binding sites and enhances docking reliability. Although M3R structure (5ZHP) is retrieved from Rattus norvegicus due to non-availability of human

crystal structure, its selection is still acceptable due to high sequence similarity between rat and human M3R proteins, especially at the active binding site (Venter et al. 1984).

The detailed docking study emphasizes strong and specific interactions between chosen ligands and target proteins. The successful validation of docking protocol, as confirmed by RMSD values below 2.0 Å for both targets 8WE8 and 5ZHP, ensures its accuracy and reliability(Hadni and Elhallaoui 2020). This close agreement between experimental and redocked poses of co-crystallized ligands indicates that the docking protocol can efficiently reproduce experimentally obtained binding confirmations in subsequent computational analysis of selected compounds. Detailed docking study including visualization of interactions demonstrated the CPD1 as a remarkably promising candidate due to high affinity and good structural compatibility with binding sites of Cav1.2 and M3R. The strong affinity of CPD1 with Cav1.2 is confirmed by presence of hydrogen bond with residue MET1509 and multiple hydrophobic interactions with important residues (Bulusu and Desiraju2020). Additionally, presence of hydrophobic interactions with key residues at the active site of M3R further supported its dual target potential. Another promising candidate was found to be CPD7 which is supported by its good binding affinity, short and strong hydrogen bond (2.0 Å) with TYR509 in M3R. Hydrogen bonds below 2.5 Å length are considered strong and are generally related with stable ligand–protein complexes and efficient binding at proteins active sites (Herschlag and Pinney 2018). CPD9 also demonstrated good binding affinity for both targets supported by only hydrophobic interactions. Stabilizing energetically favored ligands depends heavily on weak intermolecular interactions like hydrophobic interactions (Patil et al. 2010).CPD11 and CPD19 have shown comparatively low binding affinity with target proteins, although presence of specific hydrogen bonds with key residues such as TYR529 and MET1509 indicated proper positioning within the active sites of target proteins. The involvement of the same key amino acid residues in the binding pocket like the ones interacting with co-crystallized inhibitors, further supports the probability of effective inhibition. Overall, the occurrence of hydrogen bonding and hydrophobic interactions at the recognized binding site, along with favorable binding energies,suggests that the compounds (especially CPD1 and CPD7) have the potential to modulate GIT motility through dual mechanisms.

Drug discovery is aided by timely prediction of pharmacokinetic characteristics (absorption, distribution, metabolism, excretion) and toxicity properties of compounds (Rehman et al. 2018). The absorption prediction of the selected compounds by pkCSM revealed high intestinal absorption, supported by Caco-2 permeability values, especially for CPD9. These results support their potential for oral administration. Higher VDss values for CPD9 and CPD19 indicate their wider tissue distribution, while high BBB permeability values for compound CPD9 suggested its penetration into central nervous system which is undesirable in case of antispasmodic drug candidate. The inhibition of CYP2D6 by compounds CPD9 and CPD19 may cause drug-drug interactions, while all other compounds have predicted no inhibition of both CYP2D6 and CYP3A4, indicating less probability of metabolic drug-drug interactions (Martin and Fay 2001).Compound CPD7 was predicted to have rapid clearance as indicated by higher total clearance value, while CPD1 may have slow clearance rate. All compounds were predicted to have no mutagenicity and cardiotoxicity except CPD9 showed hepatotoxic nature. Overall, compounds CPD1, CPD7, and CPD11 demonstrated balanced pharmacokinetic and toxicity profiles with fewer toxicity concerns, while CPD9 and CPD19 may need further optimization to alleviate potential toxicity risks.These resultshighlight the importance of integrating pharmacokinetic and toxicity calculations with docking and QSAR outcomes for the recognition of promising lead compounds.

The prediction of drug-likeness of compounds indicates that all the selected compounds possess physicochemical characteristics required for oral drug candidates, as demonstrated by compliance of compounds to Lipinski and Veber criteria (Bickerton et al. 2012). The consistent bioavailability score (0.55) across all studied compounds implies moderate oral bioavailability potential. The analysis of synthetic accessibility score has shown that compounds CPD11 and CPD19 are comparatively easy to synthesize chemically, whereas CPD1 may involve additional complex synthetic routes.Notably, the lack of PAINS alerts among all compounds is a positive indicator, indicating that their predicted bioactivities are less likely to be false positives. Overall, all compounds exhibited favorable drug-likeness profiles, while CPD1, instead of strong predicted bioactivity, may need further optimization due to its higher synthetic complexity and structural alerts.

Despite the promising results obtained, certain limitations should be acknowledged. Although QSAR analysis was based on experimentally derived data, which may establish variations based on different labs conditions and assays, external validation is required for further supporting predictive certainty. Although docking studies are informative, they rely on static protein structures and do not completely portray dynamic structural changes or solvent effects. Future studies including molecular dynamics simulation study, extended network pharmacology analysis, and in vitro/in vivo authentication will be important to confirm the therapeutic potential of the studied compounds

CONCLUSION

The findings of the study reveal that phytocompounds from *Mentha royleana* have potential to modify GIT motility via dual target mechanism including Cav1.2 and M3R. Among the studied compounds, CPD1 appears to be most promising lead, indicating an optimum balance of predicted biological activity, binding interactions, and electronic properties. Mutually, these findings propose that *M. royleana*is a potential source of antispasmodic

metabolites, with in silico prioritization supports its pharmacological significance and justify the need of further experimental validation and structural optimization for drug development.

REFERENCES

1. Acosta-Murillo, R., Ortiz-Bayliss, J.C. and Zapata-Morin, P.A., 2026. Enhancing cancer drug discovery: QSAR modeling with machine learning and chemical representations. *Plos one*, *21*(3), p.e0343654.
2. Ahmad, S., Jose da Costa Gonzales, L., Bowler-Barnett, E.H., Rice, D.L., Kim, M., Wijerathne, S., Luciani, A., Kandasaamy, S., Luo, J., Watkins, X. and Turner, E., 2025. The UniProt website API: facilitating programmatic access to protein knowledge. *Nucleic acids research*, 53(W1), pp.W547-W553.
3. Ambudkar, I.S., 2009. Unraveling smooth muscle contraction: the TRP link. *Gastroenterology*, 137(4), pp.1211-1214.
4. Anwar, F., Abbas, A., Mehmood, T., Gilani, A.H. and Rehman, N.U., 2019. Mentha: A genus rich in vital nutra-pharmaceuticals—A review. *Phytotherapy Research*, *33*(10), pp.2548-2570.
5. Barkun, A. and Leontiadis, G., 2010. Systematic review of the symptom burden, quality of life impairment and costs associated with peptic ulcer disease. *The American journal of medicine*, *123*(4), pp.358-366.
6. Bickerton, G.R., Paolini, G.V., Besnard, J., Muresan, S. and Hopkins, A.L., 2012. Quantifying the chemical beauty of drugs. *Nature chemistry*, *4*(2), pp.90-98.
7. Biovia, D.S., 2017. Discovery studio visualizer. *San Diego, CA, USA*, *936*, pp.240-249.
8. Bulusu, G. and Desiraju, G.R., 2020. Strong and weak hydrogen bonds in protein–ligand recognition. *Journal of the Indian Institute of Science*, *100*(1), pp.31-41.
9. Burley, S.K., Bhikadiya, C., Bi, C., Bittrich, S., Chen, L., Crichlow, G.V., Christie, C.H., Dalenberg, K., Di Costanzo, L., Duarte, J.M. and Dutta, S., 2021. RCSB Protein Data Bank: powerful new tools for exploring 3D structures of biological macromolecules for basic and applied research and education in fundamental biology, biomedicine, biotechnology, bioengineering and energy sciences. *Nucleic acids research*, 49(D1), pp.D437-D451.
10. Daina, A., Michielin, O. and Zoete, V., 2017. SwissADME: a free web tool to evaluate pharmacokinetics, drug-likeness and medicinal chemistry friendliness of small molecules. *Scientific reports*, 7(1), p.42717.
11. DeLano, W.L., 2002. The PyMOL molecular graphics system. *http://www. pymol. org/*.
12. Farnsworth, N.R., Akerele, O., Bingel, A.S., Soejarto, D.D. and Guo, Z., 1985. Medicinal plants in therapy. *Bulletin of the world health organization*, *63*(6), p.965.
13. Feng, T., Zhou, Y., Lv, B. and Cai, L., 2024. Tongxieyaofang decotion alleviates IBS by modulating CHRM3 and gut barrier. *Drug design, development and therapy*, pp.3191-3208.
14. Flaskerud, J.H., 2020. Gastric ulcers, from psychosomatic disease to infection. *Issues in Mental Health Nursing*, *41*(11), pp.1047-1050.
15. Frevel, C. and Nihan, C., 2012. *Purity and the forming of religious traditions in the ancient Mediterranean world and ancient Judaism* (Vol. 3). Brill.
16. Gao, S., Yao, X., Chen, J., Huang, G., Fan, X., Xue, L., Li, Z., Wu, T., Zheng, Y., Huang, J. and Jin, X., 2023. Structural basis for human Cav1. 2 inhibitions by multiple drugs and the neurotoxin calciseptine. *Cell*, *186*(24), pp.5363-5374.
17. Gaulton, A., Hersey, A., Nowotka, M., Bento, A.P., Chambers, J., Mendez, D., Mutowo, P., Atkinson, F., Bellis, L.J., Cibrián-Uhalte, E. and Davies, M., 2017. The ChEMBL database in 2017. *Nucleic acids research*, 45(D1), pp.D945-D954.
18. Ghosh, S., Alkawadri, T., McGarvey, L.P., Hollywood, M.A., Thornbury, K.D. and Sergeant, G.P., 2025. Role of voltage-gated Ca2+ channels and Ano1 Ca2+-activated Cl− channels in M2 muscarinic receptor-dependent contractions of murine airway smooth muscle. *American Journal of Physiology-Lung Cellular and Molecular Physiology*, *328*(2), pp.L301-L312.
19. Hadni, H. and Elhallaoui, M., 2020. 3D-QSAR, docking and ADMET properties of aurone analogues as antimalarial agents. *Heliyon*, 6(4).
20. Hagar, M., Ahmed, H.A., Aljohani, G. and Alhaddad, O.A., 2020. Investigation of some antiviral N-heterocycles as COVID 19 drug: molecular docking and DFT calculations. *International Journal of Molecular Sciences*, *21*(11), p.3922.
21. Herschlag, D. and Pinney, M.M., 2018. Hydrogen bonds: simple after all?. *Biochemistry*, 57(24), pp.3338-3352.
22. Hu, M., Fang, H., Hu, Y., Lu, C., Chen, Y., Zhong, Z., Shi, H. and Wang, Q., 2024. An Unusual Cause of Intestinal Ulcers Masquerading as Inflammatory Bowel Disease: A Case Report of Allied Disorders of Hirschsprung's Disease. *Journal of Inflammation Research*, pp.3093-3099.
23. Hussain, A.O., Hassan, A.Y., Abdel-Aziem, A. and Abou-Amra, E.S., 2025. Synthesis, antimicrobial evaluation, and computational investigation of new triazine-based compounds via DFT and molecular docking. *Scientific Reports*.
24. Igarashi-Hisayoshi, Y., Ihara, E., Bai, X., Higashi, C., Ikeda, H., Tanaka, Y., Hirano, M., Ogino, H., Chinen, T., Taguchi, Y. and Ogawa, Y., 2023. Determination of region-specific roles of the M3 muscarinic acetylcholine receptor in gastrointestinal motility. *Digestive Diseases and Sciences*, *68*(2), pp.439-450.
25. Kalgutkar, A.S., 2011. Handling reactive metabolite positives in drug discovery: What has retrospective structure–toxicity analyses taught us?. *Chemico-biological interactions*, *192*(1-2), pp.46-55.

26. Khan, B.A.B.A.R., Abdukadir, A., Qureshi, R. and Mustafa, G.H.U.L.A.M., 2011. Medicinal uses of plants by the inhabitants of Khunjerab National Park, Gilgit, Pakistan. *Pak J Bot*, *43*(5), pp.2301-2310.
27. Kim, S., Chen, J., Cheng, T., Gindulyte, A., He, J., He, S., Li, Q., Shoemaker, B.A., Thiessen, P.A., Yu, B. and Zaslavsky, L., 2021. PubChem in 2021: new data content and improved web interfaces. *Nucleic acids research*, 49(D1), pp.D1388-D1395.
28. Lagunin, A.A., Lisitsa, E.Y., Rudik, A.V., Ivanov, S.M., Dmitriev, A.V., Muraviova, E.S., Filimonov, D.A. and Poroikov, V.V., 2025. QSAR Modeling for Predicting IC50 and GI50 Values for Human Cell Lines Used in Toxicological Studies. *International Journal of Molecular Sciences*, *26*(24), p.12063.
29. Liu, H., Hofmann, J., Fish, I., Schaake, B., Eitel, K., Bartuschat, A., Kaindl, J., Rampp, H., Banerjee, A., Hübner, H. and Clark, M.J., 2018. Structure-guided development of selective M3 muscarinic acetylcholine receptor antagonists. *Proceedings of the National Academy of Sciences*, 115(47), pp.12046-12050.
30. McQuaid, K.R., 2018. Drugs used in the treatment of gastrointestinal diseases. *Basic and clinical pharmacology*, *10*, pp.1029-35.
31. Milivojevic, V. and Milosavljevic, T., 2020. Burden of gastroduodenal diseases from the global perspective. *Current Treatment Options in Gastroenterology*, *18*(1), pp.148-157.
32. Morris, G.M., Huey, R., Lindstrom, W., Sanner, M.F., Belew, R.K., Goodsell, D.S. and Olson, A.J., 2009. AutoDock4 and AutoDockTools4: Automated docking with selective receptor flexibility. *Journal of computational chemistry*, 30(16), pp.2785-2791.
33. Mou, M., Zhang, Y., Qian, Y., Zhou, Z., Liao, Y., Niu, T., Hu, W., Chen, Y., Jiang, R., Zhao, H. and Dai, H., 2025. druglikeFilter 1.0: An AI powered filter for collectively measuring the drug-likeness of compounds. *Journal of pharmaceutical analysis*, *15*(6), p.101298.
34. Narayanan, M., Reddy, K.M. and Marsicano, E., 2018. Peptic ulcer disease and Helicobacter pylori infection. *Missouri medicine*, *115*(3), p.219.
35. Neese, F., 2025. Software update: The ORCA program system—version 6.0. Wiley Interdisciplinary Reviews: Computational Molecular Science, 15(2), p.e70019.
36. O'Boyle, N.M., Banck, M., James, C.A., Morley, C., Vandermeersch, T. and Hutchison, G.R., 2011. Open Babel: An open chemical toolbox. *Journal of cheminformatics*, *3*(1), p.33.
37. Patel, H.M., Noolvi, M.N., Sharma, P., Jaiswal, V., Bansal, S., Lohan, S., Kumar, S.S., Abbot, V., Dhiman, S. and Bhardwaj, V., 2014. Quantitative structure–activity relationship (QSAR) studies as strategic approach in drug discovery. *Medicinal chemistry research*, *23*(12), pp.4991-5007.
38. Patil, R., Das, S., Stanley, A., Yadav, L., Sudhakar, A. and Varma, A.K., 2010. Optimized hydrophobic interactions and hydrogen bonding at the target-ligand interface leads the pathways of drug-designing. *PloS One*, 5(8), 2029.
39. Pereira da Silva, E.A., Martín-Aragón Baudel, M., Navedo, M.F. and Nieves-Cintrón, M., 2022. Ion channel molecular complexes in vascular smooth muscle. *Frontiers in Physiology*, *13*, p.999369.
40. Phatak, S.V. and Heble, M.R., 2002. Organogenesis and terpenoid synthesis in Mentha arvensis. *Fitoterapia*, *73*(1), pp.32-39.
41. Pires, D.E., Blundell, T.L. and Ascher, D.B., 2015. pkCSM: predicting small-molecule pharmacokinetic and toxicity properties using graph-based signatures. *Journal of medicinal chemistry*, *58*(9), pp.4066-4072.
42. Rehman, N.U., Abed, R.M., Hussain, H., Khan, H.Y., Khan, A., Khan, A.L., Ali, M., Al-Nasri, A., Al-Harrasi, K., Al-Rawahi, A.N. and Wadood, A., 2018. Anti-proliferative potential of cyclotetrapeptides from Bacillus velezensis RA5401 and their molecular docking on G-protein-coupled receptors. *Microbial Pathogenesis*, 123, 419-425.
43. Schrodinger, L.L.C., 2015. The PyMOL molecular graphics system. Version, 1, p.8.
44. Soares, T.A., Nunes-Alves, A., Mazzolari, A., Ruggiu, F., Wei, G.W. and Merz, K., 2022. The (Re)-Evolution of Quantitative Structure–Activity Relationship (QSAR) studies propelled by the surge of machine learning methods. *Journal of Chemical Information and Modeling*, *62*(22), pp.5317-5320.
45. Tanahashi, Y., Komori, S., Matsuyama, H., Kitazawa, T. and Unno, T., 2021. Functions of muscarinic receptor subtypes in gastrointestinal smooth muscle: a review of studies with receptor-knockout mice. *International journal of molecular sciences*, *22*(2), p.926.
46. Trott, O. and Olson, A.J., 2010. AutoDock Vina: improving the speed and accuracy of docking with a new scoring function, efficient optimization, and multithreading. *Journal of computational chemistry*, *31*(2), pp.455-461.
47. Venter, J.C., Eddy, B., Hall, L.M. and Fraser, C.M., 1984. Monoclonal antibodies detect the conservation of muscarinic cholinergic receptor structure from Drosophila to human brain and detect possible structural homology with alpha 1-adrenergic receptors. *Proceedings of the National Academy of Sciences*, *81*(1), pp.272-276.
48. Wegener, J.W., Schulla, V., Koller, A., Klugbauer, N., Feil, R. and Hofmann, F., 2006. Control of intestinal motility by the Ca v 1.2 L-type calcium channel in mice. *FASEB journal*, *20*(8).
49. Zheng, Y., Gao, Z., Sun, L., Shi, J., Song, J. and Ye, W., 2025. Calcium and Gastrointestinal Disorders: Mechanistic Insights and Therapeutic Interventions. *International Journal for Vitamin and Nutrition Research*, 95(5), p.39241.